CONVECTIVE PATTERNS IN LIQUID CRYSTALS DRIVEN BY ELECTRIC FIELD

An overview of the onset behaviour

Agnes Buka
Research Institute for Solid State Physics and Optics of the Hungarian Academy of Sciences
H-1525 Budapest, POB. 49, Hungary
ab@szfki.hu

Nándor Éber
Research Institute for Solid State Physics and Optics of the Hungarian Academy of Sciences
H-1525 Budapest, POB. 49, Hungary
eber@szfki.hu

Werner Pesch
Institute of Physics, University of Bayreuth
D-95440 Bayreuth, Germany
Werner.Pesch@uni-bayreuth.de

Abstract A systematic overview of various electric-field induced pattern forming instabilities in nematic liquid crystals is given. Particular emphasis is laid on the characterization of the threshold voltage and the critical wavenumber of the resulting patterns. The standard hydrodynamic description of nematics predicts the occurrence of striped patterns (rolls) in five different wavenumber ranges, which depend on the anisotropies of the dielectric permittivity and of the electrical conductivity as well as on the initial director orientation (planar or homeotropic). Experiments have revealed two additional pattern types which are not captured by the standard model of electroconvection and which still need a theoretical explanation.

Keywords: Pattern formation, instabilities, liquid crystals, electroconvection

Introduction

Patterns formed in non-equilibrium systems are fascinating objects, which arise in many physical, chemical and biological systems [1]. *Liquid crystals*,

the other key word in the title, are substances with captivating properties [2–4] and their study has made amazing progress - both in basic research and applications - in the past couple of years. How do the two subjects join and *why are liquid crystals especially attractive for studying pattern formation*? An attempt will be made in this tutorial review to answer these questions to some extent.

Pattern forming phenomena in liquid crystals can be divided into two groups. *In the first one*, liquid crystals replace isotropic fluids in the study of well known classical phenomena like Rayleigh-Benard convection, Taylor vortex flow, viscous fingering, free solidification from melt, directional solidification etc. [5]. This gives a possibility to extend the investigations from simple isotropic systems to more complex, partially ordered media. As liquid crystals are intrinsically anisotropic substances, unusual nonlinear couplings (e.g. electro-mechanical, thermo-mechanical, rotation-flow) of the hydrodynamic variables become possible. They induce various focussing effects (heat, light or charge) which in many cases give rise to considerably lower values of the external control parameters at the onset of the instability.

In the second group we find pattern forming phenomena based on new instability mechanisms arising from the specific features of liquid crystals, which have no counterpart in isotropic fluids or at least are difficult to assess. Some examples are shear (linear, elliptic, oscillatory, etc.) induced instabilities, transient patterns in electrically or magnetically driven Freedericksz transitions, structures formed in inhomogeneous and/or rotating electric or magnetic fields, electroconvection (EC), etc. [5–7].

Liquid crystals have become an important paradigm to study generic aspects of pattern forming mechanisms. Besides their stability the large aspect ratios of the typical convection cells allows the observation of extended regions with regular roll patterns. The patterns are easy to visualize by exploiting the birefringence of liquid crystals. It is convenient, that the number of accessible control parameters is larger than in standard isotropic systems. For instance, one can easily tune magnetic fields or the amplitude and the frequency of an applied voltage. It is also not difficult to change the symmetry of a convection layer via the boundary conditions or the amount of anisotropy by changing the temperature, in order to observe the effect of a transition from an isotropic to an anisotropic pattern forming system. In general one might state that liquid crystals have just the right amount and right kind of complexity and non-linearity, to make them so attractive. The understanding of patterns in liquid crystals has immensely benefitted from a close collaboration between experimentalists and theoreticians. Though the hydrodynamic description of liquid crystals may look prohibitively complex in fact a quantitative description of experiments has been achieved in many cases. In addition universal aspects of pattern forma-

tion can be addressed more easily in some cases (e.g. in terms of amplitude equations) than in isotropic systems [8].

The overview is organized as follows. In section **1** we outline briefly the relevant properties of liquid crystals and sketch the theoretical description. In section **2** we discuss electroconvection for different material parameter sets and geometries focusing mainly on the onset of convection. A summary concludes the paper.

1. Physical properties of nematics

The term *liquid crystals* denotes a family of mesophases, which consist of elongated (or sometimes oblate) molecules. They are characterized by a long range *orientational order* of the molecular axes. The resulting preferred direction in the system is described by the director field $\mathbf{n}$ (with $\mathbf{n} \cdot \mathbf{n} = 1$). The various mesophases differ in the positional order of the constituent molecules. Quite often one finds with decreasing temperature a multi-step transition from the fluid-like, random positional ordering of nematic liquid crystals (nematics) through several, layered structures to smectic liquid crystals (smectics) possessing short range crystalline order. In the following we will constrain ourselves to the highest-symmetry liquid crystalline phase, the nematic, which is the simplest representative of anisotropic uniaxial liquids.

The thermodynamical equilibrium of nematics would correspond to a spatially uniform (constant $\mathbf{n}(\mathbf{r})$) director orientation. External influences, like boundaries or external fields, often lead to spatial distortions of the director field. This results in an *elastic* increment, f_d, of the volume *free energy* density which is quadratic in the director gradients [2, 3]:

$$f_d = \frac{1}{2}K_1(\nabla \cdot \mathbf{n})^2 + \frac{1}{2}K_2(\mathbf{n} \cdot (\nabla \times \mathbf{n}))^2 + \frac{1}{2}K_3(\mathbf{n} \times (\nabla \times \mathbf{n}))^2. \qquad (1)$$

Here K_1, K_2 and K_3 are elastic moduli associated with the three elementary types of deformations; splay, twist and bend, respectively. Though the three elastic moduli are of the same order of magnitude; the ordering $K_2 < K_1 < K_3$ holds for most nematics. As a consequence of the orientational elasticity a local restoring torque (later referred to as elastic torque) acts on the distorted director field which tends to reduce the spatial variations.

In most experiments (and applications) a nematic layer is sandwiched between two solid (glass) surfaces supporting transparent electrodes. Special *surface* coatings and/or treatments allow to control the director *alignment* at the bounding plates. There are two basic geometries; the *planar* one where $\mathbf{n}$ is parallel to the surfaces (usually along $\hat{\mathbf{x}}$), and the *homeotropic* one where $\mathbf{n}$ is normal to them (along $\hat{\mathbf{z}}$). In most cases the interaction between the liquid crystal and the surface is strong enough to inhibit a change of the direction of $\mathbf{n}$ at the boundaries (strong anchoring) despite director gradients in the bulk. The

surface treatments combined with the elastic torques originating from Eq. (1) ensure the initial homogeneous (i.e. no spatial variations in the plane of the layer) director alignment of liquid crystal cells.

Due to their orientational order nematics are *anisotropic* substances, therefore in contrast to isotropic fluids many physical quantities have to be described by tensors [2, 3]. As nematics are non-chiral they exhibit an inversion symmetry as well as a cylindrical symmetry around the director. In addition, they are characterized by a non-polar molecular packing; thus the nematic phase is invariant against the transformation $\mathbf{n} \rightarrow -\mathbf{n}$. These symmetries imply that the dielectric susceptibility $\boldsymbol{\epsilon}$, the electrical conductivity $\boldsymbol{\sigma}$ and magnetic susceptibility $\boldsymbol{\chi}$ tensors each have only two different components in their principal-axis system: $\epsilon_{\parallel}$, $\sigma_{\parallel}$, $\chi_{\parallel}$ and $\epsilon_{\perp}$, $\sigma_{\perp}$, $\chi_{\perp}$ respectively. The dielectric displacement $\mathbf{D}$ induced by an electric field $\mathbf{E}$ is for instance given as $\mathbf{D} = \epsilon_{\perp}\mathbf{E} + \epsilon_{\mathbf{a}}\mathbf{n}(\mathbf{n} \cdot \mathbf{E})$. Analogous relations connect the electric current $\mathbf{j}$ to $\mathbf{E}$, and the magnetization with a magnetic field, respectively. The difference $\epsilon_a = \epsilon_{\parallel} - \epsilon_{\perp}$ defines the anisotropy of the dielectric susceptibility. Substances both with $\epsilon_a > 0$ and with $\epsilon_a < 0$ can be found among nematics, moreover, the sign may change with the frequency and/or the temperature in some compounds (at optical frequencies always $\epsilon_a > 0$). Though liquid crystals are intrinsically insulators, they usually contain (or are intentionally doped with) some ionic impurities which lead to a finite electric conductivity. In most cases the anisotropy of the electrical conductivity $\sigma_a = \sigma_{\parallel} - \sigma_{\perp}$ is positive; in other words charges are easier transported parallel to the mean orientation (director $\mathbf{n}$) of the elongated nematic molecules than perpendicular. In the layered smectic phases, on the contrary, typically $\sigma_a < 0$. In some liquid crystals with a nematic-to-smectic phase transition, when decreasing the temperature, pre-transitional fluctuations induce a sign change of σ_a already in the nematic temperature range. The anisotropy of the magnetic susceptibility $\chi_a = \chi_{\parallel} - \chi_{\perp}$ is positive for the majority of nematics due to saturated aromatic rings as main building blocks of the constituent molecules. The few exceptions with $\chi_a < 0$ are composed of exclusively non-aromatic (e.g. cyclohexane) rings.

The sign of the anisotropies ϵ_a and χ_a governs the behaviour of the liquid crystal in an electric ($\mathbf{E}$) or a magnetic field ($\mathbf{H}$) field via an *electromagnetic* contribution, f_{em}, to the *orientational free energy* density:

$$f_{em} = -\frac{1}{2}\epsilon_o\epsilon_a(\mathbf{n} \cdot \mathbf{E})^2 - \frac{1}{2}\mu_o\chi_a(\mathbf{n} \cdot \mathbf{H})^2. \qquad (2)$$

As a result, for $\epsilon_a > 0$ or $\chi_a > 0$ the electromagnetic torque tends to align the director along the fields, while in the case of $\epsilon_a < 0$ or $\chi_a < 0$ an orientation perpendicular to the field directions is preferred [2, 3, 9]. This behaviour establishes the basic working principles of most liquid crystalline electro-optic devices (displays). Though Eq. (2) indicates a similarity between the behaviour in electric and magnetic fields, one crucial difference should be pointed out. As

χ_a is of the order of 10^{-6} in SI units, distortions of the constant applied magnetic field when the director varies in space, can safely be neglected. In the electric case, however, ϵ_a is usually of the order of unity, and then the electric field distortions have to be taken into account.

Though nematics are non-polar substances, a polarization may emerge in the presence of director gradients, even in the absence of an electric field. This *flexoelectric polarization* [2, 3]

$$\mathbf{P}_{fl} = e_1\mathbf{n}(\nabla\cdot\mathbf{n}) + e_3(\mathbf{n}\cdot\nabla)\mathbf{n} \tag{3}$$

originates in the shape anisotropy of the molecules. As the flexoelectric coefficients e_1 and e_3 of rod-like nematic molecules are usually quite small, their contribution

$$f_{fl} = -\mathbf{P}_{fl}\cdot\mathbf{E} \tag{4}$$

to the free energy density is negligible in the majority of cases or is only detectable under special conditions.

Though the free energy considerations introduced above are sufficient to describe static orientational deformations in nematics, they cannot provide information about the dynamical properties of the system (e.g. the rate of reorientation upon a change of an external field). Usually dynamics involves *material flow* which couples to the director field. In the standard nemato-electrohydrodynamic theory the flow field $\mathbf{v}$ is described by a Navier-Stokes equation, which besides the elastic and viscous stresses includes the Coulomb force of an electric field on charges present. The nematic anisotropy is manifested in a complex form of the viscous stress tensor, such that the effective viscosity depends on the director orientation and the gradients of the velocity field components, which appear for instance in the strain tensor $\nabla\otimes\mathbf{v}$. The *dynamics of the director* $\mathbf{n}$ in liquid crystals is governed by a balance-of-torques principle, which involves besides the elastic and electromagnetic torques additional viscous ones in the presence of shear flow. It follows directly from standard symmetry arguments [2, 3, 10] that the complicated viscous behaviour of nematics (reorientation of the director induces flow and vice versa, flow aligns the director) can be described by eight phenomenological transport coefficients - the Ericksen-Leslie *viscosity coefficients* α_1, ..., α_6, and the rotational viscosities γ_1 and γ_2 - though in fact only 5 of them are independent (for their definitions and the relations among them refer to e.g. [2, 3, 10]). In the nemato-electrohydrodynamic model nematics are treated as ohmic conductors. To describe the *dynamics of the charge density* $\rho = \nabla\cdot\mathbf{D}$, which is coupled via $\mathbf{D} = \boldsymbol{\epsilon}\cdot\mathbf{E}$ to the electric field $\mathbf{E}$, the quasi-static approximation of the Maxwell equations is sufficient in our case, which is equivalent to the charge conservation:

$$\frac{d\rho}{dt} + \nabla\cdot\mathbf{j} = 0 \tag{5}$$

with the electric current $\mathbf{j} = \boldsymbol{\sigma} \cdot \mathbf{E}$.

The *optical properties* of nematics correspond to those of uniaxial crystals [11]. The director defines the local optical axis. The most obvious indication of the anisotropy of nematics is their birefringence. Composed of elongated molecules their extraordinary refractive index n_e is always bigger than the ordinary one n_o, i.e. nematics have a positive optical anisotropy $n_a = n_e - n_o$. When light is passing through a nematic layer, an optical path difference

$$\Delta s = \int \big[n_{eff}(z) - n_o\big] dz \tag{6}$$

between the ordinary and extraordinary rays builds up, which depends on the local director orientation. The effective refractive index $n_{eff}(z)$ for the light of extraordinary polarization decreases with increasing angle between the director and the light polarization ($n_o \leq n_{eff}(z) \leq n_e$). If placed between crossed polarizers, variation of Δs results in changes of colour and/or the intensity of the transmitted light. This feature makes the polarising microscope a standard tool for studying the textures of nematic liquid crystals.

There are, however, conditions where modulation of the optical properties can be detected with a single or without any polarizer. This occurs if the director has a spatial tilt modulation periodic in a direction perpendicular to the light path (e.g. in electroconvection). The extraordinarily polarized light then senses the ensuing periodic modulation of the refractive index n_{eff}, so the sample acts like an array of lenses. The illuminating light is focused and defocused, respectively, which results in a sequence of alternating dark and bright stripes in a properly adjusted microscope. This technique, which is used in majority of experiments, is known as the *shadowgraphy* [12, 13]. In this setup of course no intensity modulation exists when illuminated with light of ordinary polarization (n_o is constant per definition). Using unpolarized light the intensity modulations remain visible, however, the contrast is reduced since only part of the light with the appropriate polarization will contribute.

Besides microscopy *diffraction* opens another possibility to analyze periodic patterns. The modulation of the refractive index is equivalent to an optical grating, thus illuminating with a laser beam the fringe pattern of the diffraction can be detected at a distant screen. This allows determination of the pattern wavelength as well as monitoring the pattern amplitude via the fringe intensities (see [14] and references therein).

All the physical parameters mentioned above are material specific and temperature dependent (for a detailed discussion of the material properties of nematics, see for instance [4]). Nevertheless, some general trends are characteristic for most nematics. Increasing the temperature the absolute values of the anisotropies usually decrease, until they drop to zero at the nematic-isotropic phase transition. The electrical conductivities increase with increasing temper-

ature as well, while the viscosity coefficients decrease. If the substance has a smectic phase at lower temperatures, some pre-transitional effects may be expected already in the nematic phase. One example has already been mentioned when discussing the sign of σ_a. Another example is the divergence of the elastic modulus K_2 close to the nematic-smecticA transition since the incipient smectic structure with an orientation of the layers perpendicular to $\mathbf{n}$ impedes twist deformations.

2. Electroconvection

Convection instabilities driven by temperature gradients are common in nature. They are for instance crucial ingredients for the dynamics of our atmosphere and drive the earth dynamo. They present an intensively studied paradigm for the dynamics of extended nonlinear systems with many degrees of freedom and show clearly the typical bifurcation sequences: spontaneous pattern formation by destabilization of the *homogeneous basic state* $\rightarrow$ *complex patterns (secondary bifurcations)* $\rightarrow$ *chaos/turbulence*. The understanding of such systems has been in particular promoted by laboratory experiments in the buoyancy driven classical Rayleigh-Benard convection in a layer of a simple fluid heated from below [15]. Already this experiment allows a wide range of possible modifications like rotating or inclining the experimental setup or the use of more complex working fluids like binary fluids or electrically conducting liquid metals. The wealth of phenomena are still far from being exhausted, either from the experimental or from the theoretical point of view.

Electrically driven convection in nematic liquid crystals [6, 7, 16] represents an alternative system with particular features listed in the Introduction. At onset EC represents typically a regular array of convection rolls associated with a spatially periodic modulation of the director and the space charge distribution. Depending on the experimental conditions the nature of the roll patterns changes, which is reflected in particular in the wide range of possible wavelengths λ found. In many cases λ scales with the thickness d of the nematic layer, therefore it is convenient to introduce a dimensionless wavenumber as $q = \frac{2\pi}{\lambda}\frac{d}{\pi}$ which will be used throughout the paper. Most of the patterns can be understood in terms of the Carr-Helfrich (CH) mechanism [17, 18] to be discussed below, from which the standard model (SM) has been derived [19]. Some scenarios fall outside that frame and need obviously new, other mechanism(s) for description.

Experiments and theoretical considerations have shown that the key parameters are the symmetry of the system (planar or homeotropic boundary conditions), the dielectric and the conductivity anisotropies. It is therefore convenient to categorize the various combinations as listed in Table 1. In its last

column the structures predicted and/or observed are summarized which will be discussed below systematically.

Table 1. Eight different combinations (labelled **A** to **H**) of initial director alignments and the sign of anisotropies ϵ_a, σ_a. The EC pattern species are characterized in the last column: CH stands for patterns, which are compatible with the Carr-Helfrich mechanism, in contrast to the remaining, nonstandard ones (ns-EC)

Case	Alignment	ϵ_a	σ_a	Type of transition
A	planar	< 0	> 0	direct CH, ns-EC (prewavy)
B	homeotropic	> 0	< 0	direct CH
C	homeotropic	< 0	> 0	secondary CH, ns-EC (prewavy)
D	planar	> 0	< 0	secondary CH
E	planar	> 0	> 0	direct CH, Freedericksz
F	homeotropic	> 0	> 0	direct CH (α-induced)
G	planar	< 0	< 0	direct CH (α-induced), ns-EC (longitudinal)
H	homeotropic	< 0	< 0	direct CH, Freedericksz, ns-EC (longitudinal)

First we discuss configurations which can be described by the standard model where patterns appear either directly or as a secondary instability (section **2.1**). Then we discuss briefly EC phenomena not covered by the standard model (section **2.2.**).

2.1. Standard EC based on the Carr-Helfrich mechanism

EC is typically driven by an ac voltage. Its amplitude is used as the main control parameter, while the driving frequency provides a convenient second control parameter. Two types of modes, the *conductive* and the *dielectric*, are allowed by symmetry (see the generic stability diagram sketched in Fig. 1). In the low-frequency, conductive regime the director and the flow field are practically time independent, while the electric field follows the external driving in time; in the high-frequency dielectric regime (for frequencies above the so-called cut-off frequency f_c, which increases with decreasing charge relaxation time $\tau_q = \frac{\epsilon_o \epsilon_\perp}{\sigma_\perp}$) the situation is reversed. In the following we will mostly focus on the conductive regime.

EC occurs in a layer (parallel to the $x-y$ plane) of homogeneously aligned nematics in the presence of an electric field across the layer (along the $\hat{\mathbf{z}}$ axis). To describe the convecting state one needs the velocity field $\mathbf{v}(\mathbf{r},t)$, the director field $\mathbf{n}(\mathbf{r},t)$ and the charge distribution $\rho(\mathbf{r},t)$ (or the electric potential $\phi(\mathbf{r},t)$ inside the layer), which are available from the nemato-hydrodynamic equations described in section **1**. These coupled partial differential equations cannot be solved analytically with the realistic rigid boundary conditions (vanishing $\mathbf{v}$, fixed $\mathbf{n}$ and ϕ at the confining plates). Typically investigations of

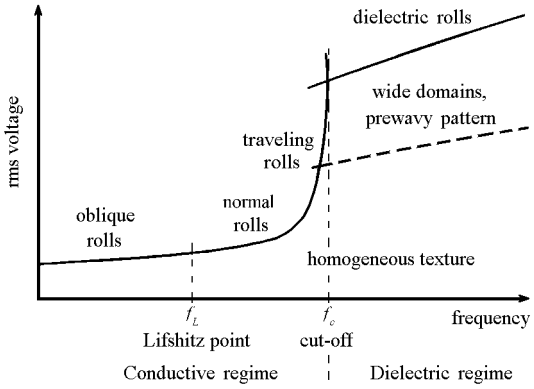

Figure 1. Schematic morphological phase diagram in the $U - f$ plane. Solid lines correspond to the threshold voltage of standard electroconvection, the dashed line denotes the threshold of the prewavy patterns or wide domains (see later). For details see [16].

EC start with a linear stability analysis of the basic homogeneous state, which yields the threshold voltage $U_c(f)$ and the critical wavenumber $q_c(f)$ as function of frequency. Much insight into the mechanisms of EC has been obtained by deriving approximate, analytical expressions for the critical quantities U_c and q_c. This development started with the seminal work of Carr [17] and Helfrich [18] in the planar geometry. They extracted the basic positive feedback mechanism responsible for EC, which is now called the 'Carr-Helfrich (CH) mechanism' in the literature: any director fluctuation leads to charge separation, flow is excited due to the Coulomb force in the Navier-Stokes equation. The flow exerts a viscous torque on the director reinforcing its initial fluctuation and thus the charge density. The mechanism is opposed by viscous damping of the flow and the elastic torques, such that EC appears only above a certain threshold voltage.

The original, so called 1-d formula of Carr and Helfrich, has been later refined and generalized into a 3-d theory capable to calculate the wavevector and describe real, three dimensional patterns (like normal or oblique rolls), other geometries and the dielectric regime [16].

Approximate analytical threshold formulas (examples are shown in Eqs. (7) and (8)) have been very useful not only to interpret specific experiments but also to get insight into general trends. For instance it can be shown that the CH mechanism remains unaltered if all three key parameters, the initial director alignment, ϵ_a and σ_a, are 'reversed' simultaneously, i.e. the change planar $\rightarrow$ homeotropic is combined with a sign reversal of ϵ_a and σ_a. In fact pairs of systems connected by this reversal transformation (cases **A**↔**B**, **C**↔**D**, **E**↔**H** and **F**↔**G** in Table 1) show close similarities.

In the following, first, the situations will be discussed where EC occurs as a primary forward bifurcation and where the standard model is directly applicable (cases **A** and **B**). Then we discuss configurations where EC sets in as a secondary instability upon an already distorted Freedericksz ground state and compare with experiments (cases **C** and **D**). Note that in this case already the linear analysis based on the standard model becomes numerically demanding. Finally we address those combinations of parameters where a direct transition to EC is not very robust, since it is confined to a narrow ϵ_a range around zero. For cases **E** and **H** this range may be accessible experimentally while for cases **F** and **G** it is rather a theoretical curiosity only.

Case A: planar alignment, $\epsilon_a < 0$ & $\sigma_a > 0$. This is the most studied, classical case, since the conductivity anisotropy of usual nematics (substances without a smectic phase) is typically positive. Concerning ϵ_a there is a big choice of materials with negative dielectric anisotropy.

The starting point is the analytical expression for the *neutral curve* in planar alignment with realistic rigid boundary conditions in the conductive regime [20]:

$$U^2(q,f) = \frac{\pi^2 K^{eff}}{\epsilon_o \epsilon_a^{eff} + I_h \frac{(\alpha_3/q^2 - \alpha_2)\tau_q \sigma_a^{eff}}{\eta^{eff}}} \tag{7}$$

with the overlap integral $I_h = 0.97267$ and $\tau_q = \epsilon_o \epsilon_\perp / \sigma_\perp$ the charge relaxation time, which decreases with increasing $\sigma_\perp$. The effective material parameters $K^{eff} > 0$, $\epsilon_a^{eff} < 0$, $\sigma_a^{eff} > 0$, $\eta^{eff} > 0$ are proportional to the corresponding physical quantities (elastic moduli, dielectric and conductivity anisotropies and viscous damping coefficients respectively). The effective values are frequency (f) and wavenumber (q) dependent (for the complete expressions see [20]). Eq. (7) has been derived with the use of a truncated Galerkin expansion: each variable is represented by *one test function* with respect to z which fulfills the boundary conditions and possesses the appropriate symmetry. The minimum of $U(q,f)$ with respect to q yields the critical wavenumber $q_c(f)$ which determines the threshold voltage $U_{th}(f) = U(q_c, f)$.

In Eq. (7) one can easily identify the impact of the various terms: on increasing either the orientational elasticity (K^{eff}), or the dielectric torques (ϵ_a^{eff}) (which both tend to turn back the director to the initial homogeneous alignment) or the viscous damping of the flow (η^{eff}) the threshold increases. The only destabilizing term, which is responsible for the onset of the patterning ($q \neq 0$) instability, is the CH term, $(\alpha_3/q^2 - \alpha_2)\tau_q \sigma_a^{eff}$ (note $\alpha_2 < 0$ and $|\alpha_3| \ll |\alpha_2|$).

The important role played by the electrical conductivity anisotropy σ_a is evident: if it decreases, $U^2(q,f)$ increases and diverges at a small positive value of σ_a when the two terms in the denominator compensate each other.

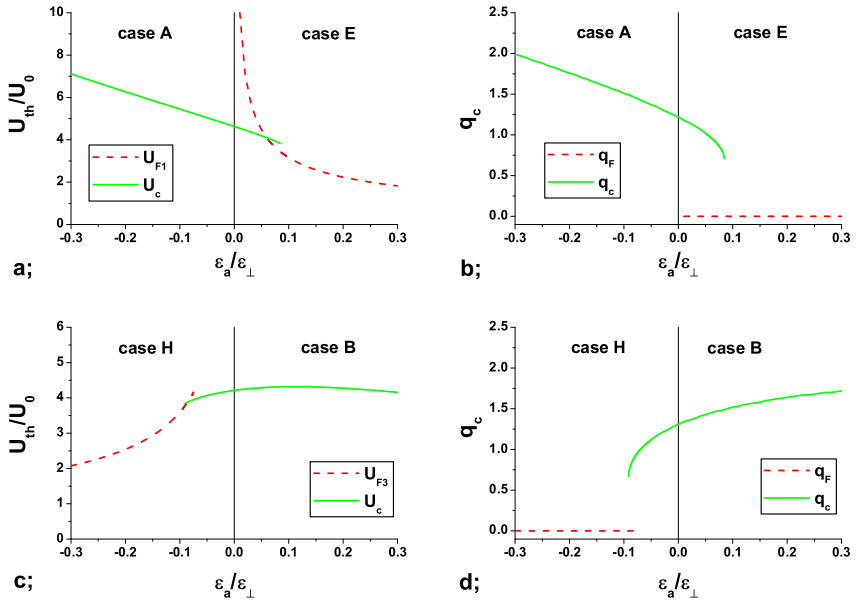

Figure 2. Threshold voltage U_{th}/U_0 and the critical wavenumber q_c versus the dimensionless dielectric anisotropy $\varepsilon_a/\varepsilon_\perp$ calculated from Eqs. (7) and (8). a; b; Planar alignment with $\sigma_a > 0$, c; d; homeotropic alignment with $\sigma_a < 0$. Dashed lines correspond to the Freedericksz transition, solid lines to the direct EC transition.

If σ_a approaches zero or becomes negative (case **F**) the CH term vanishes or acts stabilizing, respectively; thus convection is not expected. The role of ϵ_a is somewhat different: an EC transition exists for vanishing and even for positive ϵ_a (case **E**).

When analyzing the frequency dependences $U_{th}(f)$ and $q_c(f)$ it is obvious from Eq. (7) in line with general symmetry arguments that both quantities start with zero slope at $f = 0$. They increase monotonically with f and diverge at the cutoff frequency f_c, where the dielectric regime takes over. For simplicity we restrict the detailed presentation of the threshold behaviour to the limit $f \to 0$ and to MBBA material parameters [2, 4, 19] except that we allowed for variations of ϵ_a (while keeping $\epsilon_\perp$ constant) and reversed the sign of σ_a for the cases **B**, **D**, **G** and **H**.

In Fig. 2 the results for the critical voltage U_{th} (left panels, in units of $U_0 = \sqrt{\pi^2 K_1/(\epsilon_o \epsilon_\perp)}$, $U_0 = 1.19$V for MBBA parameters) and the corresponding critical wavenumber q_c (right panels) are summarized as function of $\epsilon_a/\epsilon_\perp$. The data are barely distinguishable from results of a rigorous linear stability analysis based on the full standard model [21].

In case **A** (left panels of Fig. 2a-b) $U(q)$ has only one minimum at a finite q_c, both $U_c(\epsilon_a)$ and $q_c(\epsilon_a)$ are almost linearly decreasing functions. EC sets in in the whole $\epsilon_a < 0$ range at a few Volts applied to the convection cell.

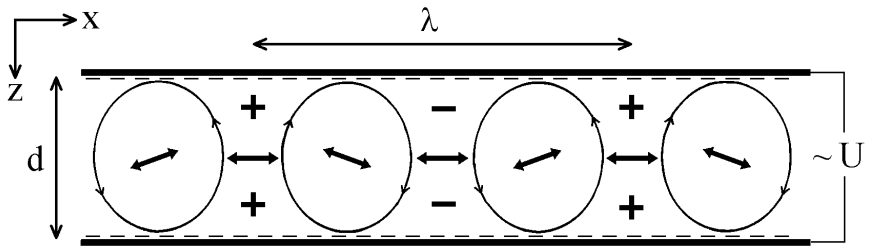

Figure 3. Cross section of a roll pattern at the direct onset to EC in the planar geometry (indicated by the small dashes at the confining plates). Double arrows denote the director modulations, which are maximal at the midplane. The lines follow the stream lines. The symbols $+$ and $-$ denote the sign of the induced charges, shown at a phase of the applied ac voltage where the electric field points downward.

Figure 3 exhibits the director and charge distribution and the velocity field in the $x-z$ plane at onset of electroconvection, where the $\hat{\mathbf{x}}$ direction is parallel to the initial (planar) director alignment, λ is the pattern wavelength.

Experiments carried out on MBBA, I52 and Merck Phase 4 and 5 [22–25] match typically very well the quantitative calculations of the stability diagram. Often oblique rolls (see Fig. 4a), where the wavevector of the striped patterns makes a nonzero angle with the basic director alignment, appear in the conductive regime below a Lifshitz point ($f < f_L$) and normal rolls (Fig. 4b) above it. Their wavelengths λ are of the order of the cell thickness d. The dielectric rolls (Fig. 4c) appearing at frequencies above the cut-off ($f > f_c$) can be normal or oblique, however their wavelength is independent of d and is usually $3-4\mu$m. The patterns are regular (the snapshot in Fig. 4c was taken at a higher voltage above threshold in order to have a higher contrast to the expense of producing defects due to secondary bifurcations) and have a large aspect ratio.

For completeness we note that in many cases in experiments traveling rolls (Hopf bifurcation) have been observed at onset usually at the high frequency end of the conductive range (see Fig. 1). The phenomenon has withstood theoretical understanding for a long time, until the standard model has been generalized in a way that the simple ohmic conductivity was replaced by ionic mobilities. The resulting weak electrolyte model (WEM) [26, 27] provided an explanation and good quantitative agreement with experiments in MBBA [28], I52 [24] and Phase 5 [29].

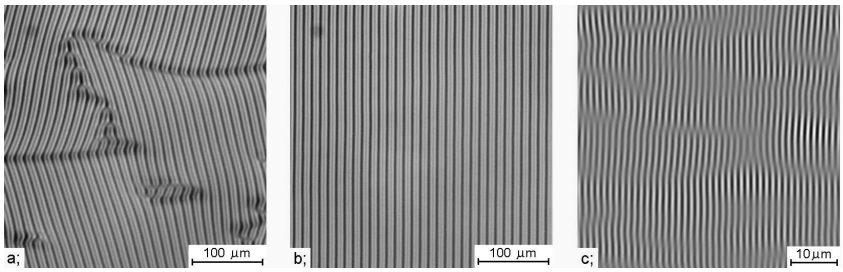

Figure 4. Snapshots of EC patterns slightly above onset for case **A** taken in a polarizing microscope with a single polarizer (shadowgraph images, Phase 5, $d = 9\mu$m). a; Oblique rolls, b; normal rolls, c; dielectric rolls (Note the difference in magnification.). The initial director orientation is horizontal. The contrast was enhanced by digital processing.

Also shown by the dashed line in Fig. 1 is the experimental threshold curve for prewavy patterns or wide domains ($\lambda \approx 4 - 10d$) which represent also electroconvecting structures though not captured by the standard model (see later in Section **2.2.**).

Case B: homeotropic alignment, $\epsilon_a > 0$ & $\sigma_a < 0$. Here the initial director orientation and the sign of both anisotropies are reversed compared to case **A**.

Recent work showed [30] that EC sets in here with a continuous transition from the homogeneous state directly, similarly to the classical configuration of case **A**. It has been shown that the pattern forming mechanism including the role of the elastic, dielectric, viscous and CH terms is analogous and the standard model is applicable. The analytical one-mode neutral-curve expression for homeotropic initial alignment [31] reads as follows:

$$U^2(q,f) = \frac{\pi^2 K^{eff}}{-\epsilon_o \epsilon_a^{eff} - I_h \frac{(\alpha_3 - \alpha_2/q^2)\tau_q \sigma_a^{eff}}{\eta^{eff}}} \,. \tag{8}$$

It is similar to Eq. (7), however, the effective quantities and τ_q appearing in Eq. (8) are differently defined. In fact they can be transformed into each other by interchanging the subscripts $\| \leftrightarrow \perp$ and the material parameters $K_1 \leftrightarrow K_3$, $\eta_1 \leftrightarrow \eta_2$ and $\alpha_2 \leftrightarrow -\alpha_3$. These transformations are natural consequences of switching the boundary conditions between planar and homeotropic.

The right hand side of Eq. (8) is positive for $\epsilon_a > 0$ and $\sigma_a < 0$ (case **B**). One expects for $U_c(\epsilon_a)$ and $q_c(\epsilon_a)$ similar functions (mirror images) to those of case **A**. However the corresponding plots shown in Fig. 2 look somewhat different. This is due to the asymmetry of the scaling factors (we plot in all cases ϵ_a in units of $\epsilon_\perp$ and U_{th} in units of $U_0 = \sqrt{\pi^2 K_1/\epsilon_o \epsilon_\perp}$).

The essential difference between cases **A** and **B** lies in the symmetry of the system. In case **A** the planar geometry is anisotropic, the wavevector direction is selected by the boundary conditions. In contrast, the homeotropic alignment in case **B** provides isotropic conditions in the plane of the patterns and the direction of the wavevector of the striped patterns is chosen accidently at threshold, which corresponds to a spontaneous breaking of the rotational symmetry.

The director field and charge distribution as well as the velocity fields are sketched in Fig. 5 for the homeotropic case. The director tilt angle is determined by the applied voltage, but, as already stressed before, the azimuthal angle is not selected in this isotropic configuration. As will be demonstrated below, this freedom leads easily to disordered patterns with slow variations of the azimuthal director component in the weakly nonlinear regime.

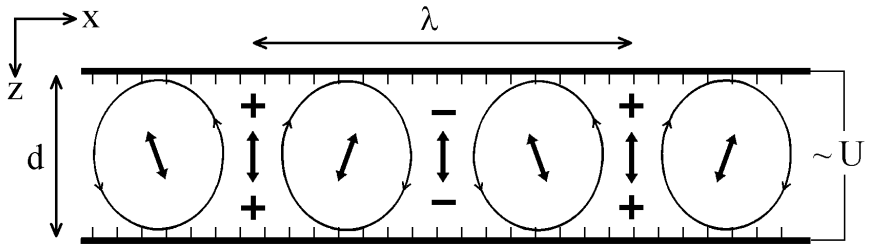

Figure 5. Cross section of a roll pattern at the direct onset of EC in the homeotropic geometry (indicated by the small dashes at the confining plates). Double arrows denote the director modulations, which are maximal at the midplane. Thin lines are for the flow field. The symbols $+$ and $-$ denote the sign of the induced charges.

Experiments have been carried out on p-(nitrobenzyloxy)-biphenyl [30] and typical patterns in the conductive range at onset are shown in Fig. 6. At low frequencies disordered rolls without point defects have been observed with a strong zig-zag (ZZ) modulation (see Fig. 6a) which can be interpreted as the isotropic version of oblique rolls. Above a critical frequency a square pattern is observed which retains the ZZ character, because the lines making up the squares are undulated. At onset the structure is disordered, however, after a transient period defects are pushed out and the structure relaxes into a nearly defect free, long-wave modulated, quasi-periodic square pattern (see Fig. 6b).

The $U_c - f$ phase diagram is similar to Fig. 1 and can quantitatively be reproduced by the standard model. The dielectric regime has not been seen experimentally that may have purely technical reasons (there is no argument to exclude the dielectric regime). Regarding the various patterns in the nonlinear regime they have been well reproducible by a suitable weakly nonlinear anal-

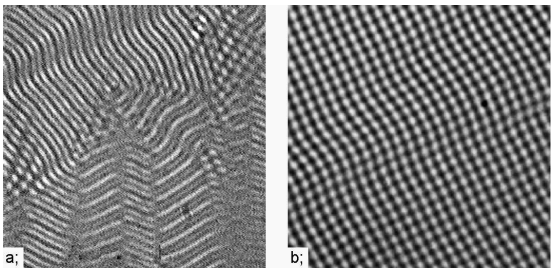

Figure 6. Snapshots of EC patterns slightly above onset for case **B**. a; ZZ modulated disordered rolls, b; undulated (soft) squares.

ysis [32, 33]. In contrast to the generalized Ginzburg-Landau amplitude equations usually used in the anisotropic regimes, a generalized Swift-Hohenberg model had to be constructed here.

Case C: homeotropic alignment, $\epsilon_a < 0$ & $\sigma_a > 0$. In this combination of the material parameters the linear stability analysis of the base state does not predict a direct transition to EC since the resulting expression for $U^2(q)$ in Eq. (8) is negative for all $q \neq 0$ (except for ϵ_a in the immediate vicinity of zero, see below). The reason is that the two terms in the denominator act differently compared to the case **B** ($\epsilon_a > 0$, $\sigma_a < 0$) described in the previous subsection. The Carr-Helfrich torque is now stabilizing while the dielectric torque ($\propto \epsilon_a^{eff}$) acts destabilizing. At $q = q_F = 0$ this term dominates and describes at the threshold U_{F3} (see Fig. 7a) the continuous bifurcation to the homogeneous (along the $\hat{\mathbf{x}}$ direction) bend Freedericksz distorted state (see Fig. 8a).

However, in the vicinity of $\epsilon_a \approx 0$ the destabilizing influence of the CH term is restored if it becomes comparable with the ϵ_a^{eff} term. Inspection of Eq. (8) shows that this may occur at very large q: the $(\alpha_3 - \alpha_2/q^2)$ term which is large and positive for usual q ($q \approx 1$), decreases with increasing q and becomes eventually negative for materials with $\alpha_3 < 0$ if $q^2 > \alpha_2/\alpha_3$ (≈ 100 for MBBA). This results in a patterning mode with $q = q_\alpha$ against which the basic homogeneous homeotropic configuration would become unstable. This mode is only activated if its threshold U_α becomes lower than U_{F3}. U_α and U_{F3} intersect at a very small, negative $\epsilon_a/\epsilon_\perp \approx -5 \cdot 10^{-5}$ (the intersection point is not resolvable even in Fig. 7c). To the right from the intersection q_α becomes in fact the fastest growing mode [34]. Note, that this "α-induced" direct transition to EC is only an interesting theoretical possibility, with no experimental relevance, since one would need a nematic with ϵ_a almost exactly

zero and one should be able to detect patterns with extremely large q at very high U_α.

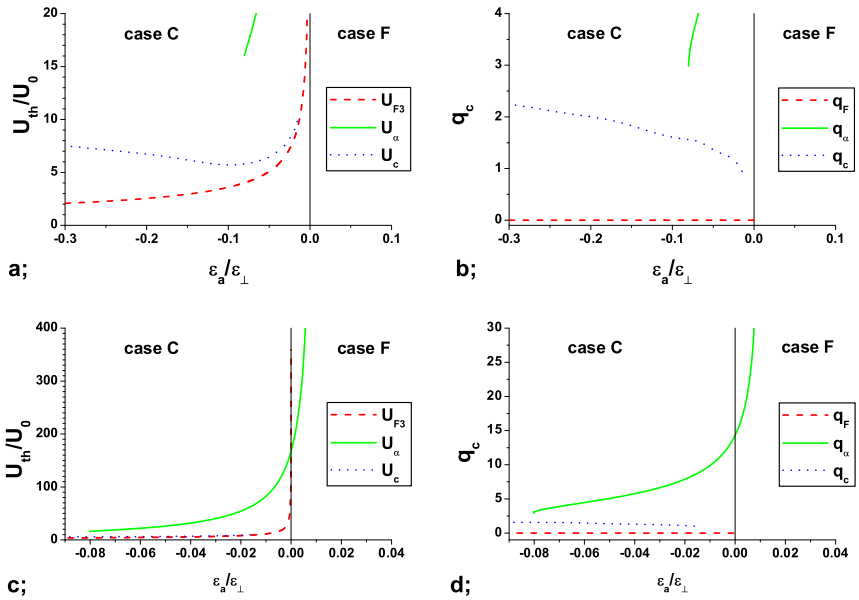

Figure 7. Threshold voltages U_{th}/U_0 and the critical wavenumber q_c versus the relative dielectric anisotropy $\varepsilon_a/\varepsilon_\perp$ calculated from Eq. 8. Homeotropic alignment with $\sigma_a > 0$. The upper (a; b;) and lower (c; d;) plots differ only in the axis scales. Dashed lines belong to the Freedericksz transition, solid lines to the direct transition to an ("α-induced") EC patterned state, dotted lines represent a secondary transition to EC.

Above the Freedericksz threshold U_{F3} the tilt angle with respect to $\hat{\mathbf{z}}$ increases with increasing voltage such that eventually one arrives practically at a planarly aligned nematic layer at the midplane. Consequently the planar CH mechanism is expected to be activated. Convection rolls are now to be superimposed on the elastically pre-distorted Freedericksz state (Fig. 8b); a simple analytical threshold formula does not exist. Thus one has to rely on a numerical linear stability analysis of the Freedericksz state in the framework of the standard model. Since boundary layers have to be resolved, one needs more $(6-8)$ Galerkin modes than typically required in the standard planar case. These numerical calculations have achieved the same good agreement with the experiments in MBBA or Phase 5 [35, 36] as before in the case of the primary bifurcations (cases **A** and **B**). U_c in Fig. 7 (a,c) and q_c in Fig. 7 (b,d) (dotted lines) represent the results of such calculations which match well the experimental data [9]. Note that the U_c and q_c curves should continue to ϵ_a almost zero; however, we have been unable to access this regime numerically,

since the minimum of the neutral curve becomes too shallow. In the range $-0.2 < \epsilon_a/\epsilon_\perp < -0.03$ a bifurcation to oblique (instead of normal) rolls occurs at threshold. This shows up as little wiggles in the slope of the modulus of the critical wavevector plotted in Fig. 7b. Recent experiments [36] have shown, however, that at certain combinations of the material parameters (e.g. for Phase 5/5A) an unusual situation occurs, namely oblique rolls become restricted to a finite $f_{L1} < f < f_{L2}$ frequency interval. Below f_{L1} normal rolls appear, and reappear above f_{L2}, i.e. there are two Lifshitz points.

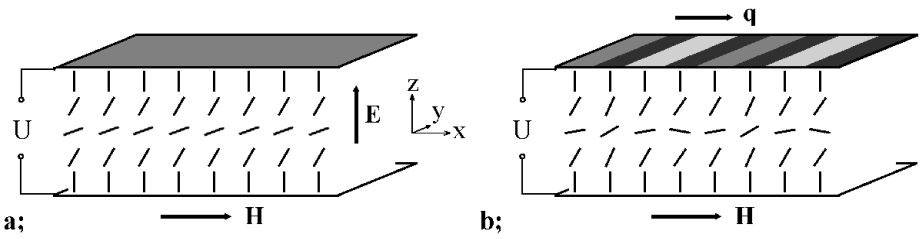

Figure 8. Schematic director profile in case **C**. a; Freedericksz distorted state, b; with superposed electroconvection pattern.

Though the initial homeotropic state is isotropic (as in case **B**), the isotropy in the plane is spontaneously broken due to the Freedericksz transition. Consequently the EC pattern is formed on an anisotropic background with a preferred direction in the $x - y$ plane (as in case **A**). The local azimuthal angle of the Freedericksz tilt direction is singled out by coincidence, thus it may vary in space as well as in time representing a soft Goldstone mode which is coupled to the EC patterning mode. As a result the patterns at onset - oblique rolls (Fig. 9a) or normal rolls (Fig. 9b) depending on the frequency - are disordered and correspond to a special manifestation of spatio-temporal chaos, the soft mode turbulence [37–39].

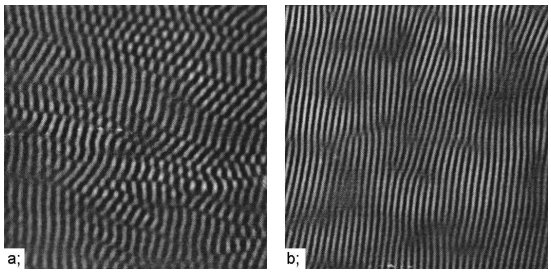

Figure 9. Snapshots of electroconvection patterns superposed on the Freedericksz state in case **C**. a; oblique rolls, b; normal rolls.

The chaotic behavior reflected in the disordered patterns can be suppressed if the initial isotropy of the homeotropic alignment is broken by applying a magnetic field $\mathbf{H}$ parallel to $\hat{\mathbf{x}}$ as shown in Fig. 8 [40]. The azimuthal angle of $\mathbf{n}$ is then singled out by the magnetic field, the patterns become nicely ordered and exhibit similar morphologies as shown in Fig. 4 for the case **A** (e.g. the disordered pattern of Fig. 9a becomes similar to that in Fig. 4a).

The homeotropic geometry offers some advantages in observing certain phenomena in the (weakly) nonlinear regime of EC (at voltages above U_c). It is known that normal rolls (NR) become unstable above a certain voltage with respect to abnormal roll (AR) modes [41], which are characterized by a rotation of the director in the $x-y$ plane, while the roll axis remains unchanged. In planar cells the polarization of light follows adiabatically the director orientation (Mauguin's principle) [2, 3]. Weak non-adiabatic effects have to be resolved in this case to detect possible in-plane rotations of the director which are maximal near the mid-plane and vanish at the boundaries.

In homeotropic cells, however, in-plane rotations of the director are reflected in a net azimuthal rotation of the optical axis (and the light polarization) across the cell which has allowed a detailed exploration of the characteristics of the NR-AR transition. Experiments have shown an excellent agreement with the predictions of generalized Ginzburg-Landau models [36].

A second example is related to the motion of defects (dislocations in the roll pattern) which constitutes the basic mechanism of wavevector selection. In the normal-roll regime the stationary structure is characterized by the condition $\mathbf{q} \parallel \mathbf{H}$. However, when changing the field direction one can easily induce a temporary wavevector mismatch $\mathbf{\Delta q} = \mathbf{q_{new}} - \mathbf{q_{old}}$ which relaxes via a glide ($\mathbf{v} \parallel \mathbf{q}$) motion of defects. Experiments have confirmed the validity of detailed theoretical predictions both with respect to the the direction ($\mathbf{v} \perp \mathbf{\Delta q}$) and the magnitude (consistent with logarithmic divergence at $|\mathbf{\Delta q}| \to 0$) of the defect velocity $\mathbf{v}$ [42].

The homeotropic geometry allows also for the appearance of structures with a secondary spatial periodicity - chevrons - in the conductive regime at voltages considerably larger than U_c [43]. Such type of chevrons, which are characterized by a periodic arrangement of defect chains, have been seen before exclusively in the dielectric regime.

Case D: planar alignment, $\epsilon_a > 0$ & $\sigma_a < 0$. This configuration is realized by 'reversing' the sign of the anisotropies and the initial director orientation compared to case **C**. Thus cases **D** and **C** belong to the same 'family', analogously to cases **B** and **A** as discussed before. The standard model applies and the theoretical analysis can be based on Eq. (7) for the neutral curve $U^2(q)$.

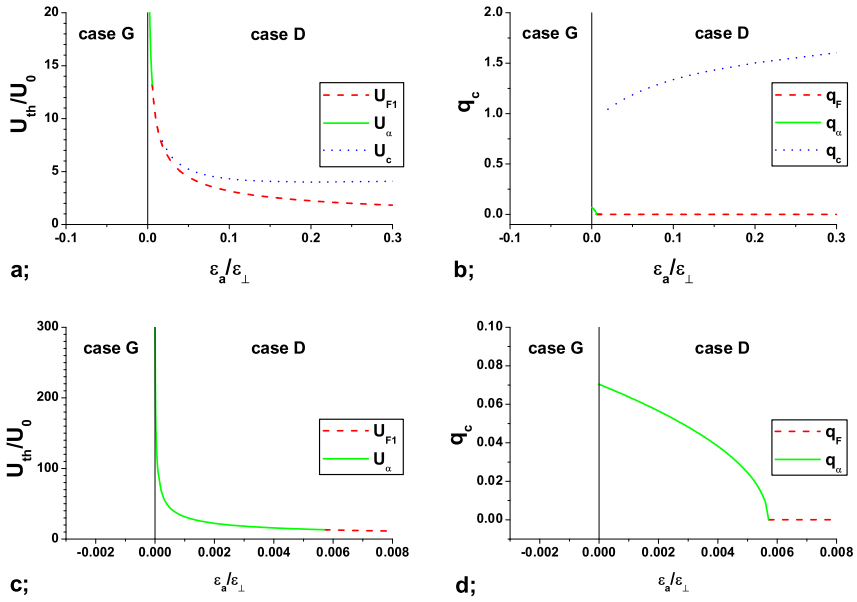

Figure 10. Threshold voltages U_{th}/U_0 and the critical wavenumber q_c versus the relative dielectric anisotropy $\varepsilon_a/\varepsilon_\perp$ calculated from Eq. (7). Planar alignment with $\sigma_a < 0$. The upper (a; b;) and lower (c; d;) plots differ only in the axis scales. Dashed lines belong to the Freedericksz transition, solid lines to the direct transition to an ("α-induced") EC patterned state. Dotted lines represent a secondary transition to EC.

Upon increasing the voltage usually the first transition is to the homogeneous ($q = q_F = 0$) splay Freedericksz state with a frequency independent threshold voltage U_{F1} (Fig. 10a), i.e the absolute minimum of the neutral curve is at $q = 0$. However, very near to $\epsilon_a = 0$ the absolute minimum appears at a finite q. Thus we have the planar counterpart of the "α-induced" EC described in case **C**. The Freedericksz threshold smoothly transforms into an EC threshold U_α at $\epsilon_a/\epsilon_\perp = 0.0057$ (see Fig. 10c-d). Below this a direct transition to EC is predicted with q_α growing continuously from zero and remaining extremely small. This transition seems to be a better candidate for experimental observation than its homeotropic counterpart, because both U_α and q_α are substantially lower than in case **C**.

For $\epsilon_a/\epsilon_\perp > 0.0057$ EC sets in superimposed onto the Freedericksz state (secondary instability) at a higher voltage $U_c > U_{F1}$. The standard model can be applied here too by carrying out numerical linear stability analysis of the Freedericksz distorted state, and one is faced with similar modifications and difficulties as mentioned in case **C** before. The ϵ_a dependence of U_c and q_c, which appear as dotted lines in Fig. 10(a-b) have been calculated numerically.

One should note that the convection rolls are now oriented parallel to the initial director alignment, contrary to the normal rolls in case **A** or **C**.

Measurements in the only available substance have presented well-aligned rolls in the whole conductive frequency range [30] similarly to case **A** (compare Fig. 11a with Fig. 4b), in fact with $\mathbf{q} \perp \mathbf{n}$ as predicted by the theory. The wavenumber scales with d^{-1}. The calculations above provided a good quantitative agreement with experiments for both $U_c(f)$ and $q_c(f)$.

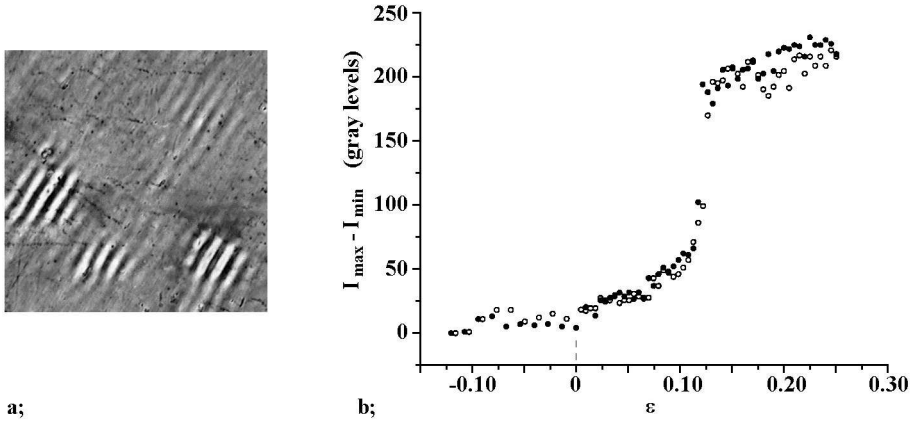

Figure 11. a; Snapshot of EC pattern in the Freedericksz distorted planar geometry of case **D**. b; Voltage dependence of the contrast (the difference of the maximum I_{max} and minimum I_{min} intensities) of the EC pattern in case **D**. $\varepsilon = (U^2 - U_c^2)/U_c^2$ is a dimensionless control parameter.

The transition was found to be mediated by nucleation and travelling of sharp fronts (Fig. 11a) indicating a backward bifurcation, though hysteresis has not been identified directly. Rather a sharp jump in the contrast (pattern amplitude) on increasing the voltage has been detected with some indications that a low contrast pattern arises already at voltages before the jump occurs in Fig. 11b. A preliminary, weakly non-linear analysis has exhibited a bifurcation, which is in fact weakly supercritical at low frequencies. Small changes of the parameters and/or additional effects not included (e.g. flexoelectricity and weak-electrolyte effects) could change it into a more expressed subcritical bifurcation [32, 33].

Case E: planar alignment, $\epsilon_a > 0$ & $\sigma_a > 0$. Here the magnitude of ϵ_a plays a role. Starting from negative values (case **A**) a direct EC threshold persists for zero and positive ϵ_a (see Eq. (7) and Fig. 2a-b). An upper limit in ϵ_a is set by the onset of the homogeneous ($q = q_F = 0$) splay Freedericksz transition at a threshold U_{F1}. The intersection of U_c and U_{F1} occurs about

$\epsilon_a/\epsilon_\perp = 0.06$, where the Freedericksz transition starts preceding the EC bifurcation. A local minimum on the neutral curve still exists at a finite q_c up to $\epsilon_a/\epsilon_\perp = 0.09$ where q_c discontinuously drops to zero. In the parameter range where $U_c \approx U_{F1}$, interesting scenarios are expected as a result of the competition between the homogeneous and the convective mode [44, 45]. As in cases **C** and **D**, we have performed a linear stability analysis of the Freedericksz distorted state, but did not find any secondary EC threshold. To understand this behavior we note that the dielectric destabilizing torque of the basic state preferring $q = 0$ prevails over the CH torque resulting in the Freedericksz transition at U_{F1}. Increasing the voltage U above U_{F1}, the tilt-angle of the director increases and reduces further the destabilizing effect of the CH term and an even higher voltage would be required for EC onset. At large enough director tilt the CH term becomes even stabilizing and the EC threshold "runs away". EC does not superimpose onto the Freedericksz state like it does in cases **C** and **D** .

Case F: homeotropic alignment, $\epsilon_a > 0$ & $\sigma_a > 0$. This is one of the rather uninteresting situations. The only transition predicted is the "α-induced" high q instability discussed in case **C** which is the primary transition in a very narrow $\epsilon_a > 0$ interval (see Fig. 7a-d). No transition has been observed experimentally for any wavenumber at any voltage.

Case G: planar alignment, $\epsilon_a < 0$ & $\sigma_a < 0$. This is the counterpart of case **F**, thus the "α-induced" low q instability discussed in case **D** theoretically persists for $\epsilon_a < 0$ but the existence range is much smaller than in case **F**. The U_α curve diverges here at $\epsilon_a/\epsilon_\perp \approx -10^{-5}$ which can not be resolved in Fig. 10c and has not been seen experimentally.

Case H: homeotropic alignment, $\epsilon_a < 0$ & $\sigma_a < 0$. Here one expects a qualitative behaviour similar to case **E**. A direct EC transition is predicted for negative ϵ_a down to $\epsilon_a/\epsilon_\perp \approx -0.1$ (see Fig. 2c-d), though there is no experimental evidence yet. For more negative ϵ_a the Freedericksz transition takes over, above which no secondary EC threshold is expected. The discussion and arguments given for case **E** apply here as well.

2.2. Non-standard EC excluded by the CH mechanism

The standard model is very powerful and as demonstrated before it describes quantitatively the EC structures at onset and also quite deeply in the nonlinear regimes. Nevertheless there are some situations (one of them is the prewavy structure mentioned under case **A**) where the standard model does not predict a bifurcation to EC, though experimental observations have clearly identified

pattern formation accompanied by convection (ns-EC) in the presence of electric fields.

Cases A and C: $\epsilon_a < 0$ & $\sigma_a > 0$. Compounds with $\epsilon_a < 0$ and $\sigma_a > 0$ are the most common examples of substances to exhibit the CH electroconvection as discussed above. In substances with higher electrical conductivity, however, occasionally another periodical stripe pattern - the *prewavy pattern* - arises already at voltages below the EC threshold voltage U_c. This pattern has been reported for homeotropic [46] (case **C**) as well as for planar cells (case **A**) and has been called wide domains [47, 48, 9]). It is characterized by a wavelength λ much larger than the sample thickness ($\lambda \approx 4 - 10d$) (Fig. 12) as well as by much longer relaxation times than those of standard EC patterns. The stripes are running perpendicular to the director, i.e. in the same direction as the conductive normal rolls. The prewavy pattern does not produce (at least near to its threshold) a shadowgraph image, it becomes visible using crossed polarizers only. This implies that the pattern is due to an azimuthal modulation of the director which is associated with flow vortices parallel to the surfaces [49] (i.e. in the $x - y$ plane in contrast to the normal rolls in CH mechanism where both the director modulation and the flow occurs in the $x - z$ plane). While the azimuthal rotation of the director is easily detectable in homeotropic samples for any d, in planar samples its visibility requires the detection of non-adiabatic corrections to the light propagation, which restricts the sample thickness.

Measurements have shown that the prewavy pattern appears in a forward bifurcation [50]. Its threshold voltage U_{pw} has a weak, nearly linear frequency dependence. It usually occurs at higher frequencies (see Fig. 1). Conductive normal rolls, dielectric rolls and the prewavy pattern may follow each other with increasing f (dielectric rolls may be skipped in compounds with higher conductivity). Near the crossover frequency f_c the conductive (or dielectric) rolls may coexist with the prewavy pattern resulting in the defect free chevron structure [51].

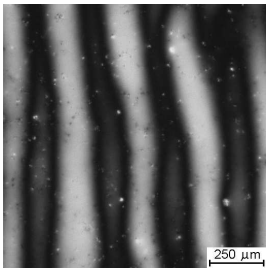

Figure 12. The prewavy pattern in homeotropic MBBA. $d = 50\mu$m.

The characteristics of the prewavy pattern which clearly differ from those of the classical EC patterns, cannot be explained using the standard model. The underlying mechanism is not yet known. One proposed interpretation - the inertial mode of EC [9] - fails to predict the correct direction of the stripes. The observation, that U_{pw} seems to remain continuous and that the flow survives when passing the nematic-to-isotropic transition with increasing temperature, may suggest that the prewavy pattern could correspond to the chevron structure of a not yet detected primary pattern created by an isotropic mechanism already at voltages below U_{pw}. However, there are no direct experimental or theoretical proofs for this idea.

Case G: planar alignment, $\epsilon_a < 0$ & $\sigma_a < 0$. Standard EC (based on the CH mechanism) is excluded for the material parameter combination $\epsilon_a < 0, \sigma_a < 0$ [2] except the 'α induced' pattern type. Nevertheless convection associated with roll formation has been observed in ac electric field in the homologous series of N-(p-n-alkoxybenzylidene)-n-alkylanilines, di-n-4-4'-alkyloxyazoxybenzenes and 4-n-alkyloxy-phenyl-4-n'alkyloxy-benzoates [52–54]. The characteristics of the patterns; i.e. the orientation of the rolls, contrast, frequency dependence of the wavevector and that of the threshold, director variation in space and time etc., are substantially different from those observed in the standard EC. Since this roll formation process falls outside of the frame of the standard model it has been called *nonstandard electroconvection* (ns-EC).

The main characteristics of these ns-EC patterns which differ from those of standard EC are:

- The overall contrast of the pattern is low compared to the standard EC structures. Near onset the ns-EC pattern is not visible with the conventional shadowgraph method, crossed polarizers are needed to detect it. Thus the director field has no z component, i.e. the director is only modulated in the $x-y$ plane. This feature also explains the low contrast.
- The threshold voltage scales with the cell thickness, thus the onset is characterized by a threshold field (not a voltage).
- The critical wavevector is perpendicular to or subtends a large angle with the initial director alignment (contrary to normal rolls) thus the rolls are parallel (longitudinal) or strongly oblique (see Fig. 13).
- The critical wavelength is comparable or larger than the cell thickness.
- The director field oscillates with the driving frequency similar as in the dielectric regime of standard EC.
- The threshold is a linear function of the driving frequency.

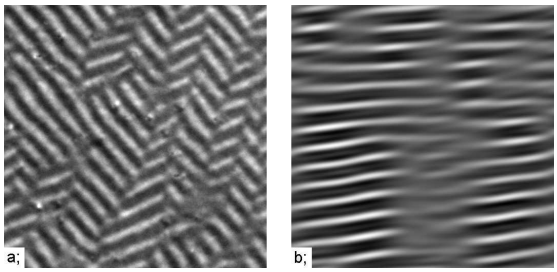

Figure 13. Snapshots of nonstandard electroconvection pattern in case **G** taken with crossed polarizers. a; Oblique rolls, b; parallel rolls. Contrast was enhanced by digital processing. The initial director orientation is horizontal. The depicted image is $0.225 \times 0.225\text{mm}^2$, $d = 11\mu$m.

As possible explanations, several ideas have been proposed: a hand-waving argument based on "destabilization of twist fluctuations" [52], a possibility of an isotropic mechanism based on the non-uniform space charge distribution along the field [53] and the flexoelectric effect [55–57].

Case H: homeotropic alignment, $\epsilon_a < 0$ & $\sigma_a < 0$. Above the Freedericksz transition, where no standard EC is predicted, convection (ns-EC) builds up with properties similar to those listed for case **G**. The patterns are disordered (see Fig. 14) as expected for an initial homeotropic alignment.

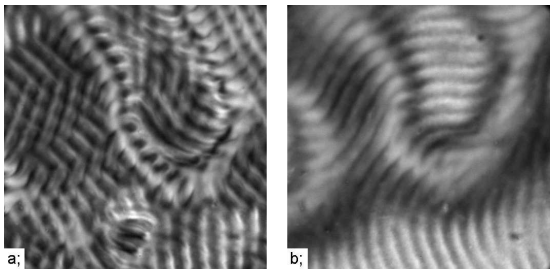

Figure 14. Snapshots of nonstandard electroconvection pattern in case **H** taken with crossed polarizers. a; Oblique rolls, b; parallel rolls. The initial director orientation is horizontal. The depicted image is $0.45 \times 0.45\text{mm}^2$, $d = 20\mu$m.

Summary

In this paper we have reviewed the structures appearing at onset of electroconvection in nematic liquid crystals. The influence of the relevant material parameters (ϵ_a and σ_a) and the role of the initial director alignment were ex-

plored. Our calculations using a linear stability analysis of the standard model of electroconvection (performed for zero frequency) revealed that four different scenarios characterized by different wavenumber ranges q can be identified: (**1**) is the $q_F = 0$ mode (a homogeneous deformation known as the *Freedericksz transition*) predicted and observed in cases **C**, **D**, **E** and **H**, which is actually a convection free state; (**2**) is the $q_c \approx 1$ mode (wavelength in the range of d), the *classical electroconvection*, appearing either as a primary or a secondary bifurcation, both have been detected and explained quantitatively in the cases **A**, **B** and **C**, **D**; (**3**) is a short wavelength structure with $q_\alpha > 15$ in case **F** and (**4**) is a long wavelength one with $q_\alpha < 0.07$ in case **D**, both are only theoretically predicted (*"α-induced" EC*) for substances with $\alpha_3 < 0$. Extending the scope from zero to low frequencies no qualitative change of the mode assortment is expected though some morphological changes of the pattern are present (oblique versus normal rolls).

At high frequencies - in the dielectric regime - Eqs. (7) and (8) do not apply. We mention for completeness that independent calculations for that range would invoke a different q-mode (**5**), the *dielectric rolls*, with a wavelength which does not scale with d.

Experiments, however, proved that further stripe patterns occur which do not have as yet an unambiguous, widely accepted interpretation. These patterns can be classified into two additional q-modes: (**6**) is the *prewavy* pattern (or wide domains) with $0.2 < q < 0.5$ observed in cases **A** and **C**, replacing or coexisting with modes (**2**) and/or (**5**); and (**7**) corresponds to the parallel (*longitudinal*) rolls which were observed in cases **G** and **H**, exhibiting $q_c \approx 1$ similarly to mode (**2**), but otherwise having different characteristics.

Acknowledgment

The authors wish to thank L. Kramer for useful discussions, E. Kochowska and A. Cauquil-Vergnes for the snapshots of ns-EC patterns. This work was supported by the EU grant EU-HPRN-CT-2002-00312, the NATO ASI 980684 and the Hungarian Research Fund OTKA T-037336.

References

[1] M.C. Cross and P.C. Hohenberg, *Rev. Mod. Phys.* **65**, 851 (1993).

[2] P.G de Gennes and J. Prost, *The Physics of Liquid Crystals*, Clarendon Press, Oxford, 1993.

[3] S. Chandrasekhar, *Liquid Crystals*, University Press, Cambridge, 1992.

[4] *Physical Properties of Liquid Crystals: Nematics*, editors: D.A. Dunmur, A. Fukuda and G.R. Luckhurst, Inspec, London, 2001

[5] *Pattern Formation in Liquid Crystals*, editors: A. Buka and L. Kramer, Springer, New York, 1996.

[6] W. Pesch and U. Behn, Electrohydrodynamic Convection in Nematics. In *Evolution of Spontaneous Structures in Dissipative Continuous Systems*, editors: F.H. Busse and S.C. Müller, pages 335–383, Springer, New York, 1998.

[7] L. Kramer and W. Pesch, Electrohydrodynamics in Nematics. In *Physical Properties of Liquid Crystals: Nematics*, editors: D.A. Dunmur, A. Fukuda and G.R. Luckhurst, pages 441–454, Inspec, London, 2001

[8] W. Pesch and L. Kramer, General Mathematical Description of Pattern-Forming Instabilities. In *Pattern Formation in Liquid Crystals*, editors: A. Buka and L. Kramer, pages 69–90, Springer, New York, 1996.

[9] L.M. Blinov and V.G. Chigrinov, *Electrooptic Effects in Liquid Crystal Materials*, Springer, New York, 1994.

[10] H. Pleiner and H. Brandt, Hydrodynamics and Electrohydrodynamics of Liquid Crystals. In *Pattern Formation in Liquid Crystals*, editors: A. Buka and L. Kramer, pages 15–68, Springer, New York, 1996.

[11] M. Born and E. Wolf, *Principles of Optics*, Pergamon, Oxford, 1996.

[12] S. Rasenat, G. Hartung, B.L. Winkler and I. Rehberg, *Exp. Fluids* **7**, 412 (1989).

[13] S. P. Trainoff and D. Canell, *Physics of Fluids* **14**, 1340 (2002).

[14] N. Éber, S.A. Rozanski, Sz. Németh, Á. Buka, W. Pesch and L. Kramer, *Phys. Rev. E* **70**, 61706 (2004).

[15] E. Bodenschatz, W. Pesch and G. Ahlers, *Annu. Rev. Fluid Mech.* **32** , 709-778 (2000).

[16] L. Kramer and W. Pesch, Electrohydrodynamic Instabilities in Nematic Liquid Crystals. In *Pattern Formation in Liquid Crystals*, editors: A. Buka and L. Kramer, pages 221–255, Springer, 1996.

[17] E.F. Carr, *Mol. Cryst. Liq. Cryst.* **7**, 253 (1969).

[18] W. Helfrich, *J. Chem. Phys.* **51**, 4092 (1969).

[19] E. Bodenschatz, W. Zimmermann and L. Kramer, *J. Phys. (Paris)* **49**, 1875 (1988).

[20] See equation (6.5) on p. 221 in [16]. Note that there $I_h = 0.97267$ has been replaced by one and that $\alpha_3/q^2 - \alpha_2$ has been approximated by $|\alpha_2|$.

[21] Numerical codes for the linear analysis of the full standard model can be obtained upon request from the authors.

[22] A. Joets and R. Ribotta, *J. Phys. (Paris)* **47**, 595 (1986).

[23] S. Kai, N. Chizumi and M. Kokuo, *Phys. Rev. A* **40**, 6554 (1989).

[24] M. Dennin, M. Treiber, L. Kramer, G. Ahlers and D. Cannell, *Phys. Rev. Lett.* **76**, 319 (1995).

[25] S. Rasenat, V. Steinberg and I. Rehberg, *Phys. Rev. A* **42**, 5998 (1990).

[26] M. Treiber and L. Kramer, *Phys. Rev. E* **58**, 1973 (1989).

[27] M. Treiber and L. Kramer, *Mol. Cryst. Liq. Cryst.* **261**, 951 (1995).

[28] I. Rehberg, S. Rasenat and V. Steinberg, *Phys. Rev. Lett.* **62**, 756 (1989).

[29] M. Treiber, N. Éber, Á. Buka and L. Kramer, *J. Phys. II (Paris)*, **7**, 649 (1997).

[30] Á. Buka, B. Dressel, W. Otowski, K. Camara, T. Tóth-Katona, L. Kramer, J. Lindau, G. Pelzl and W. Pesch, *Phys. Rev. E* **66**, 051713/1-8 (2002).

[31] See equation (6.29) on p.244 in [16], which has been rewritten. The definition of $\bar{\sigma_a}$ in equation (6.31) contains a misprint. The correct equation reads: $\bar{\sigma_a}^{(eff)} = \frac{\sigma_a(\epsilon_\perp/\epsilon_\parallel - \epsilon_a\sigma_\perp/(\epsilon_\parallel\sigma_a))}{(1+\omega'^2)\bar{S}}$.

[32] Á. Buka, B. Dressel, L. Kramer and W. Pesch, *Phys. Rev. Lett.* **93(4)**, 044502/1-4 (2004).

[33] Á. Buka, B. Dressel, L. Kramer and W. Pesch, *Chaos* **14**, 793-802 (2004).

[34] L. Kramer, A. Hertrich and W. Pesch, Electrohydrodynamic Convection in Nematics: the Homeotropic Case. In *Pattern Formation in Complex, Dissipative Systems*, editor: S. Kai, pages 238–246, World Scientific, Singapore (1992).

[35] A. Hertrich, W. Decker, W. Pesch and L. Kramer, *Phys. Rev. E* **58**, 7355 (1998).

[36] A.G. Rossberg, N. Éber, Á. Buka and L. Kramer, *Phys. Rev. E* **61**, R25 (2000).

[37] S. Kai, K. Hayashi and Y. Hidaka, *J. Phys. Chem.* **100**, 19007 (1996).

[38] Y. Hidaka, J.-H. Huh, K. Hayashi, M. Tribelsky and S. Kai, *J. Phys. Soc. Jpn.* **66**, 3329 (1997).

[39] P. Tóth, Á. Buka, J. Peinke and L. Kramer, *Phys. Rev. E* **58**, 1983 (1998).

[40] H. Richter, N. Kloepper, A. Hertrich and Á. Buka, *Europhys. Lett.* **30**, 37 (1995).

[41] H. Richter, Á. Buka and I. Rehberg, *Phys. Rev. E* **51**, 5886 (1995).

[42] P. Tóth, N. Éber, T.M. Bock, Á. Buka and L. Kramer, *Europhys. Lett.* **57**, 824 (2002).

[43] Á. Buka, P. Tóth, N. Éber and L. Kramer, *Physics Reports* **337**, 157 (2000).

[44] B. Dressel and W. Pesch, *Phys. Rev. E.* **67**, 031707 (2003)

[45] B. Dressel, L. Pastur, W. Pesch, E. Plaut and R. Ribotta, *Phys. Rev. Lett.* **88** , 024503 (2002)

[46] S. Kai and K. Hirakawa, *Solid State Commun.* **18** 1573 (1976).

[47] P. Petrescu and M. Giurgea, *Phys. Lett.* **59A**, 41 (1976).

[48] A.N. Trufanov, M.I. Barnik and L.M. Blinov, A Novel Type of the Electrohydrodynamic Instability in Nematic Liquid Crystals. in *Advances in Liquid Crystal Research and Application*, editor: L. Bata, pages 549–560, Akadémiai Kiadó - Pergamon Press (1980).

[49] J.-H. Huh, Y. Yusuf, Y. Hidaka, and S. Kai, *Mol. Cryst. Liq. Cryst.* **410**, 39 (2004).

[50] J.-H. Huh, Y. Hidaka, Y. Yusuf, N. Éber, T. Tóth-Katona, Á. Buka and S. Kai, *Mol. Cryst. Liq. Cryst.* **364**, 111 (2001).

[51] J.-H. Huh, Y. Hidaka, A.G. Rossberg and S. Kai, *Phys. Rev. E* **61**, 2769 (2000).

[52] M. Goscianski and L. Léger, *J. Phys. (Paris)* **36**, N.3, C1-231 (1975).

[53] L.M. Blinov, M.I. Barnik, V.T. Lazareva and A.N. Trufanov, *J. Phys. (Paris)* **40**, N.4, C3-263 (1979).

[54] E. Kochowska, S. Németh, G. Pelzl and Á. Buka, *Phys. Rev. E* **70**, 011711 (2004).

[55] N.V. Madhusudana and V.A. Raghunathan, *Mol. Cryst. Liq. Cryst. Lett.* **5**, 201 (1988).

[56] N.V. Madhusudana and V.A. Raghunathan, *Liquid Crystals*, **5**, 1789 (1989).

[57] M.I. Barnik, L.M. Blinov, A.N. Trufanov and B.A. Umanski, *J. Phys. (Paris)* **39**, 417-422 (1978).